www.springer.com/41230
https://doi.org/10.1007/s41230-023-1049-2
Research & Development
Vol. 20 No. 1 January 2023
CHINA FOUNDRY

# Effect of secondary aging on microstructure and properties of cast Al-Cu-Mg alloy

***Rui-ming Su[1], Yong-xin Jia[1], Jian Xiao[2], Guang-long Li[1], Ying-dong Qu[1], and Rong-de Li[1]**

*1. School of Materials Science and Engineering, Shenyang University of Technology, Shenyang 110870, China*

*2. Guizhou Yonghong Aviation Machinery Limited Liability Company, Guiyang 550009, China*

**Abstract:** To obtain better comprehensive properties of cast Al-Cu-Mg alloys, the secondary aging (T6I6) process (including initial aging, interrupted aging and re-aging stages) was optimized by an orthogonal method. The microstructures of the optimized Al-Cu-Mg alloy were observed by means of scanning electron microscopy and transmission electron microscopy, and the properties were investigated by hardness measurements, tensile tests, exfoliation corrosion tests, and intergranular corrosion tests. Results show that the S phase and θ' phase simultaneously exist in the T6I6 treated alloy. Appropriately increasing the temperature of the interrupted aging in the T6I6 process can improve the mechanical properties and corrosion resistance of Al-Cu-Mg alloy. The optimal comprehensive properties (tensile strength of 443.6 MPa, hardness of 161.6 HV) of the alloy are obtained by initial aging at 180 °C for 2 h, interrupted aging at 90 °C for 30 min, and re-aging at 170 °C for 4 h.

**Keywords:** cast Al-Cu-Mg alloy; secondary aging; mechanical properties; corrosion resistance; strengthening phase

**CLC numbers:** TG146.21 **Document code:** A **Article ID:** 1672-6421(2023)01-071-07

## 1 Introduction

Al-Cu-Mg alloys have been widely used as structural materials for the aerospace industry due to their high tensile strength, toughness and good processability [1-5]. The hardness and strength of Al-Cu-Mg alloys are low, and pitting corrosion, intergranular corrosion (IGC) and local corrosion always occur in Al-Cu-Mg alloys [6,7], which limit their industrial applications. Therefore, improving the comprehensive properties of Al-Cu-Mg alloys has always been the focus of research.

Numerous studies have shown that heat treatment can significantly enhance the properties of Al-Cu-Mg alloys [8-10]. The standard T6 process can improve the mechanical properties of Al-Cu-Mg alloys, but the improvement is limited. To further improve the mechanical properties of the alloy, Lumley et al. [11] proposed the secondary aging process. The secondary aging process means that the standard T6 process is interrupted for a period at a lower temperature. The secondary aging process is called the T6I4 or T6I6 process according to whether re-aging is carried out after low-temperature interrupted aging. The T6I6 process involves initial aging, interrupted aging and re-aging stages. A large number of studies have shown that the nucleation and growth rule of strengthening phases in alloys is changed by the secondary precipitation phenomenon in low-temperature interrupted aging [12,13]. The T6I6 process is able to improve the strength of the alloy without reducing the toughness of the alloy, and has been applied to numerous age-hardenable aluminum alloys [14-16]. Yin et al. [17] pointed out that an increase in the interrupted aging temperature may be more conducive to the secondary nucleation and improve the aging-hardening effect of the T6I6 process. Meanwhile, the secondary precipitation phenomenon in the T6I6 process also has a great effect on grain boundary precipitates. The change in grain boundary precipitates will lead to a change in corrosion resistance [18, 19]. However, the effect of the T6I6 process on the corrosion resistance of Al-Cu-Mg alloys has been seldom studied.

In this work, the T6I6 process was optimized using the orthogonal method, and the effect of the T6I6 process on the mechanical properties and corrosion resistance of cast Al-Cu-Mg alloy was also studied.

***Rui-ming Su**

Male, Ph. D., Associate Professor. His research interests mainly focus on the preparation of aluminum alloys.

E-mail: suruiming1984@163.com

**Received: 2022-06-04; Accepted: 2022-12-16**

## 2 Experimental procedure

The experimental material is a cast Al-Cu-Mg alloy with a diameter of 250 mm and 100 mm long. The composition of the Al-Cu-Mg alloy is 4.78%Cu-1.52%Mg-0.48%Mn-0.28%Fe-0.13%Si (mass fraction), and the balance is Al.

The samples were solution heat-treated at 500 °C for 40 min in a resistance furnace and then quenched rapidly. Then, the secondary aging, i.e., T6I6, was carried out. The samples were aged in a constant temperature blast drying oven for three stages. The main factors of the T6I6 process: initial aging temperature and time, interrupted aging temperature and time, and re-aging temperature and time are listed in Table 1.

The hardness test was carried out on a UH250 digital Vickers hardness tester, and the average value of each sample was calculated after five tests. Some T6I6 process parameters were determined according to the hardness of the alloy, and then further optimized. These parameters were further studied by tensile test, corrosion test and microstructure observation.

The tensile samples conforming to ISO 6892-1:2009 with a gauge length of 25 mm and diameter of 5 mm were tested by using an MTS universal tensile tester with a strain rate of $10^{-4}$ $s^{-1}$. The average value of each sample was calculated after three tests. The exfoliation corrosion (EXCO) test was carried out according to the ASTM G34-01 (2013) standard. The sample was in the shape of a rectangular prism. One surface of the sample was exposed to the solution. All other surfaces were sealed with rosin. The surface area-to-volume ratio was 25 $cm^2 \cdot L^{-1}$ during the experiment. The solution was 4 $mol \cdot L^{-1}$ NaCl+0.5 $mol \cdot L^{-1}$ $KNO_3$+0.1 $mol \cdot L^{-1}$ $HNO^3$, and the solution temperature was controlled at 25±3 °C. The samples were removed from the solution after soaking for 96 h to observe the corrosion condition, and the EXCO rating was evaluated according to the standard ASTM G34-01(2013). The IGC test was carried out according to the ASTM G110-1992(2009) standard. Three samples were taken under different heat treatment processes. The surface area-to-volume ratio of the test was less than 20 $mm^2 \cdot mL^{-1}$. The surfaces of the samples were polished with metallographic sandpaper, immersed in 10% NaOH solution for 5–15 min for pretreatment, washed with water, immersed in 30% $HNO_3$ solution until the surfaces were smooth, and then washed with water again. Finally, the samples were vertically suspended in corrosion solution (57 g NaCl and 10 mL $H_2O_2$ were dissolved in 1 L distilled water) for 6 h, and the solution temperature was 35±2 °C. At the end of the experiment, the IGC depth was observed by TM3030 scanning electron microscopy (SEM). JEM-2100 transmission electron microscopy (TEM) was used to observe the microstructure of the samples.

**Table 1: Experimental design using L25($5^6$) orthogonal method**

| No. | Initial aging | | Interrupted aging | | Re-aging | |
|---|---|---|---|---|---|---|
| | Temp. (°C) | Time (h) | Temp. (°C) | Time (min) | Temp. (°C) | Time (h) |
| | A | B | C | D | E | F |
| 1 | 150 | 1 | 80 | 10 | 150 | 1 |
| 2 | 150 | 2 | 90 | 20 | 160 | 2 |
| 3 | 150 | 3 | 100 | 30 | 170 | 3 |
| 4 | 150 | 4 | 110 | 40 | 180 | 4 |
| 5 | 150 | 5 | 120 | 50 | 190 | 5 |
| 6 | 160 | 1 | 90 | 30 | 180 | 5 |
| 7 | 160 | 2 | 100 | 40 | 190 | 1 |
| 8 | 160 | 3 | 110 | 50 | 150 | 2 |
| 9 | 160 | 4 | 120 | 10 | 160 | 3 |
| 10 | 160 | 5 | 80 | 20 | 170 | 4 |
| 11 | 170 | 1 | 100 | 50 | 160 | 4 |
| 12 | 170 | 2 | 110 | 10 | 170 | 5 |
| 13 | 170 | 3 | 120 | 20 | 180 | 1 |
| 14 | 170 | 4 | 80 | 30 | 190 | 2 |
| 15 | 170 | 5 | 90 | 40 | 150 | 3 |
| 16 | 180 | 1 | 110 | 20 | 190 | 3 |
| 17 | 180 | 2 | 120 | 30 | 150 | 4 |
| 18 | 180 | 3 | 80 | 40 | 160 | 5 |
| 19 | 180 | 4 | 90 | 50 | 170 | 1 |
| 20 | 180 | 5 | 100 | 10 | 180 | 2 |
| 21 | 190 | 1 | 120 | 40 | 170 | 2 |
| 22 | 190 | 2 | 80 | 50 | 180 | 3 |
| 23 | 190 | 3 | 90 | 10 | 190 | 4 |
| 24 | 190 | 4 | 100 | 20 | 150 | 5 |
| 25 | 190 | 5 | 110 | 30 | 160 | 1 |

## 3 Results and analysis

### 3.1 Hardness and calculated S/N values

The influence of T6I6 process factors on the hardness of Al-Cu-Mg alloy can be judged by the calculated S/N values. Table 2 lists the hardness results and S/N values. Since the experimental design is orthogonal, it is possible to separate out the effect of each T6I6 process factor at different levels [20-22]. For example, the mean S/N value for initial aging temperature at Levels 1, 2, 3, 4 and 5 can be calculated by averaging S/N values for the Experiments 1 to 5, 6 to 10, 11 to 15, 16 to 20 and 21 to 25, respectively. These results are shown in Fig. 1.

As shown in Fig. 1, with the increase of all the T6I6 process parameters, the S/N values of the hardness of the alloy firstly increase and then decrease, but the change of S/N values for the re-aging temperature is not obvious. In addition, the S/N values at the interrupted aging temperature of 80 °C, 90 °C and 100 °C are similar, which are 42.898, 43.016 and 43.046, respectively, the S/N values at the interrupted aging time of 30 min and 40 min are similar, which are 43.168 and 43.094, respectively.

### 3.2 Analysis of variance

The analysis of variance of the hardness of the alloy is listed in Table 3. The hardness of the T6I6 treated alloy is most influenced by the initial aging temperature and time, accounting for 34.90% and 36.07%, respectively; greatly influenced by the interrupted aging temperature, interrupted aging time and re-aging time, accounting for 4.20%, 17.51% and 6.66%, respectively; and less influenced by the re-aging temperature, accounting for only 0.66%.

## 4 Optimization and discussion

To further optimize the T6I6 process, it is necessary to comprehensively consider the influence of T6I6 process factors. As shown in Fig. 1, the S/N values of initial aging temperature, initial aging time and re-aging time show obvious peaks, therefore, the corresponding optimal initial parameters of 180 °C×2 h, and re-aging time of 4 h can be easily confirmed. But, the S/N values of interrupted aging temperature and time and re-aging temperature do not show obvious peaks. As shown in Table 3, the re-aging temperature has the least influence on T6I6 process, so it is not necessary to be future optimized, the parameters with the highest S/N value (170 °C×4 h) are selected. Therefore, future optimization should be focused on interrupted aging temperature (80 °C, 90 °C and 100 °C) and time (30 min and 40 min), as shown in Table 4.

**Table 2: Hardness results and calculated S/N values**

| Experiment No. | Average hardness (HV) | Calculated S/N value |
|---|---|---|
| 1 | 124.54 | 41.905957 |
| 2 | 140.42 | 42.948065 |
| 3 | 142.42 | 43.070537 |
| 4 | 134.12 | 42.549341 |
| 5 | 123.36 | 41.823051 |
| 6 | 144.26 | 43.182536 |
| 7 | 149.28 | 43.479706 |
| 8 | 138.48 | 42.827298 |
| 9 | 128.84 | 42.200335 |
| 10 | 135.68 | 42.649866 |
| 11 | 147.58 | 43.380294 |
| 12 | 144.64 | 43.205504 |
| 13 | 138.72 | 42.842670 |
| 14 | 144.78 | 43.213734 |
| 15 | 141.92 | 43.040228 |
| 16 | 144.26 | 43.182545 |
| 17 | 158.58 | 44.004822 |
| 18 | 148.54 | 43.436569 |
| 19 | 141.56 | 43.018594 |
| 20 | 138.56 | 42.832489 |
| 21 | 140.62 | 42.960670 |
| 22 | 146.00 | 43.286908 |
| 23 | 139.46 | 42.888535 |
| 24 | 132.86 | 42.467741 |
| 25 | 131.56 | 42.382277 |

### 4.1 Mechanical properties

Figure 2 shows the strain-stress curves of samples O1–O4. Table 5 lists the test results of the tensile properties and hardness of samples. It can be found that the tensile properties and hardness of the four samples show the same changing trend, and Sample O2 has the highest tensile strength, yield strength, elongation and hardness of 443.6 MPa, 401.6 MPa, 10.1% and 161.6 HV, respectively.

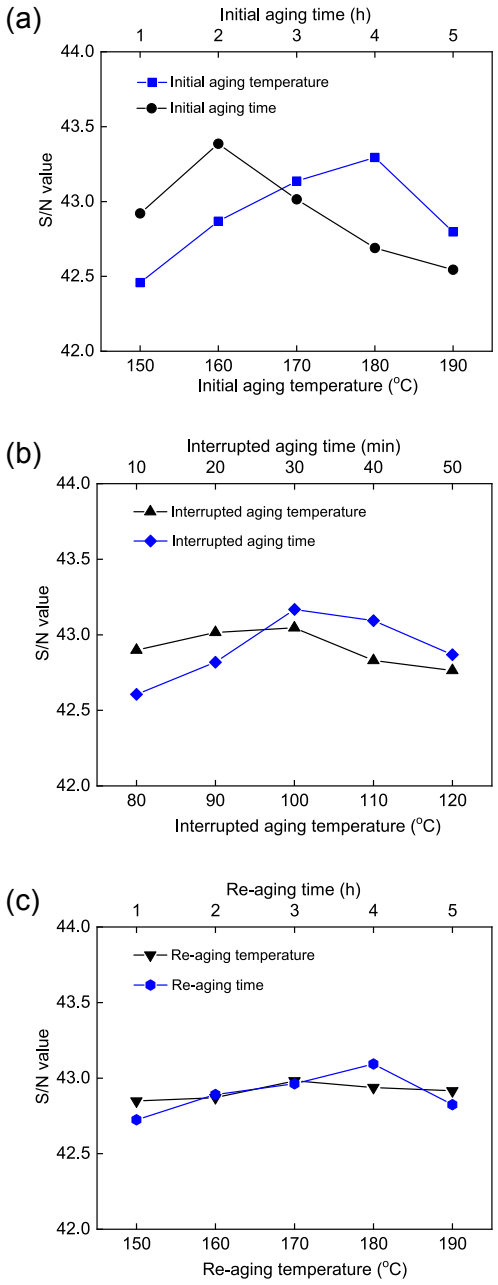


**Fig. 1: Effect of T6I6 process factors on S/N values of hardness: (a) initial aging factors; (b) interrupted aging factors; (c) re-aging factors**

Table 3: Analysis of variance of hardness of the alloys

| Factors | Degrees of freedom | Sum of square | Mean square | F-ratio | Contribution (%) |
|---|---|---|---|---|---|
| A | 4 | 528.0489 | 132.0122 | 2.374 | 34.90 |
| B | 4 | 545.7668 | 136.4417 | 2.454 | 36.07 |
| C | 4 | 63.6655 | 15.9164 | 0.286 | 4.20 |
| D | 4 | 264.8359 | 66.2090 | 1.191 | 17.51 |
| E | 4 | 10.1027 | 2.5257 | 0.045 | 0.66 |
| F | 4 | 100.6809 | 25.1702 | 0.453 | 6.66 |
| Total | 24 | 1,513.1007 | 378.2751 | 6.803 | 100 |

Table 4: Experiments corresponding to different aging treatments

| Sample | Initial aging | Interrupted aging | Re-aging |
|---|---|---|---|
| O1 | 180 °C×2 h | 80 °C×30 min | 170 °C×4 h |
| O2 | | 90 °C×30 min | |
| O3 | | 100 °C×40 min | |
| O4 | | 80 °C×40 min | |

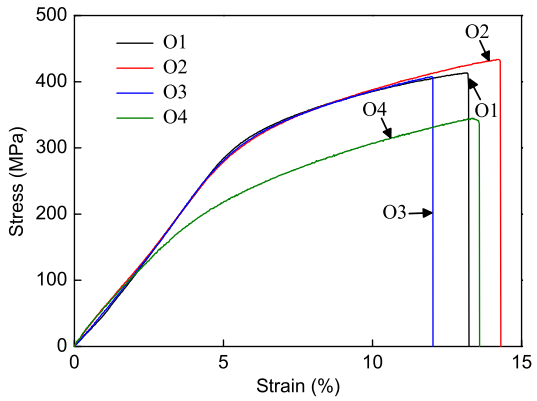


Fig. 2: Strain-stress curves of samples

Table 5: Tensile properties and hardness of samples

| Sample | Tensile strength (MPa) | Yield strength (MPa) | Elongation (%) | Hardness (HV) |
|---|---|---|---|---|
| O1 | 413.7 | 375.3 | 7.4 | 150.2 |
| O2 | 443.6 | 401.6 | 10.1 | 161.6 |
| O3 | 407.7 | 368.9 | 6.5 | 149.4 |
| O4 | 345.1 | 302.2 | 8.3 | 125.4 |

The results show that during the same aging time, appropriately increasing the low-temperature interrupted aging temperature improve the strength and hardness of the alloy. However, during the same aging temperature, the long low-temperature interrupted aging time decreases the strength and hardness.

## 4.2 Exfoliation corrosion property

The surface morphology of samples after EXCO is shown in Fig. 3. As shown in Figs. 3(a) and (d), the surfaces of samples are severely exfoliated and have been corroded to dark brown. In Fig. 3(c), a large area of exfoliation can be found on the alloy surface, which even has been decolorized to brown. In Fig. 3(b), the surface of the alloy is slightly exfoliated and decolorized, and the metallic luster still exist. Therefore, compared with other samples, the O2 sample has the slightest exfoliation degree and the smallest corroded area on the surface.

Table 6 lists the EXCO ratings of samples. It can be found that appropriately increasing the interrupted aging temperature is beneficial to improve the EXCO resistance of the alloy, but if the interrupted aging temperature is too high, the EXCO resistance of the alloy will be seriously reduced. The EXCO rating of the O2 sample is EA; its EXCO resistance is the best.

## 4.3 Intergranular corrosion property

The depth of corrosion for the alloy was further examined by IGC. Figure 4 shows the cross section morphology of samples after IGC. As shown in Fig. 4(a), corrosion develops along the grain boundaries in the O1 sample. The IGC depth of the O2 sample in Fig. 4(b) is shallower than that in Fig. 4(a). As shown in Fig. 4(c), the IGC depth of the O3 sample is the deepest and the area of corrosion is the largest. Figure 4(d) shows that the IGC depth of the alloy is shallower than that in Fig. 4(c), but the corrosion is still deep into the alloy. Table 7 lists the IGC depth of all samples, and it can be seen that the IGC depth of the O2 sample is the shallowest, which is only 105 μm.

It can be concluded that the IGC resistance of the alloy can be improved by appropriately increasing the interrupted aging temperature at the same interrupted aging time. But, too high interrupted aging temperature and too long interruption aging time will reduce the corrosion resistance of the alloy. These results are consistent with those of EXCO.

## 4.4 Microstructure analysis

Studies have shown that the precipitation sequences of Al-Cu-Mg alloys are SSS→GP zone→θ" phase→θ' phase→θ phase ($Al_2Cu$) and SSS→GPB zone→S' phase→S phase ($Al_2CuMg$) [23-26]. The bright field TEM images of all samples

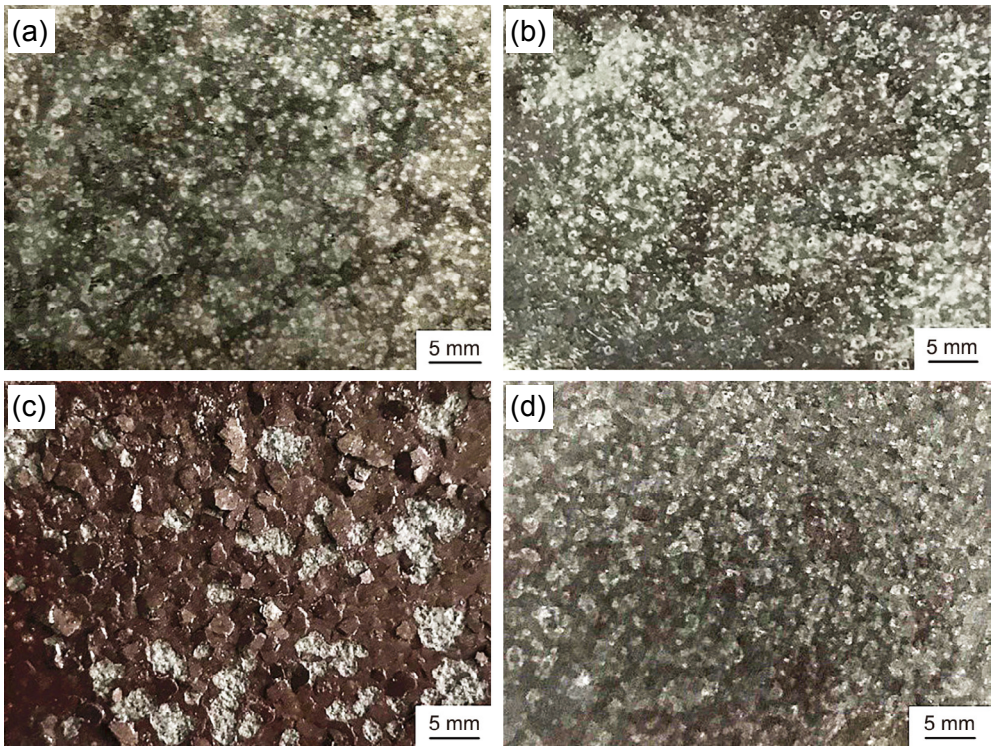


Fig. 3: EXCO surface morphology of samples: (a) O1; (b) O2; (c) O3; and (d) O4 sample

are shown in Fig. 5. It can be seen from the first four figures that the strengthening phases in the T6I6 treated alloy are S phase and θ' phase. Figure 5(a) shows that the size and distribution of S phase in the O1 sample are not uniform, and θ' phase is less. As shown in Fig. 5(b), the strengthening phases

Table 6: EXCO ratings of samples

| Sample | O1 | O2 | O3 | O4 |
|---|---|---|---|---|
| EXCO rating | EB | EA | ED | EB |

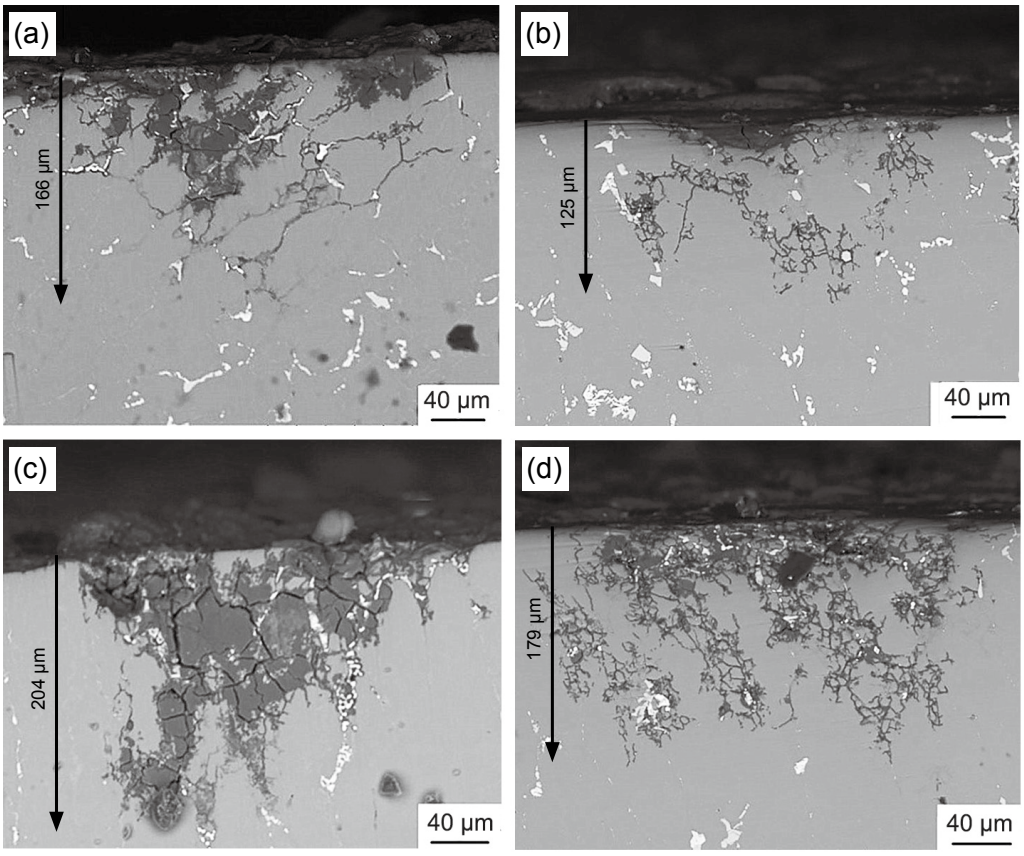


Fig. 4: IGC cross section morphology of samples: (a) O1; (b) O2; (c) O3; and (d) O4 sample

**Table 7: IGC depth of samples**

| Sample | O1 | O2 | O3 | O4 |
|---|---|---|---|---|
| IGC depth (μm) | 166 | 105 | 204 | 179 |

are uniformly distributed in the O2 sample, and most of the S phases are small (approximately 150 nm). The primary S phases in the O3 sample are severely coarsened [Fig. 5(c)], which will decrease the mechanical properties of the alloy. As shown in Fig. 5(d), the strengthening phases are uniformly distributed but slightly coarsened in the O4 sample. Figure 5(e) shows the diffraction patterns of the S phase, and the orientation relationship between the S phase and matrix is $[100]_S//[100]_{Al}$. Figure 5(f) shows the diffraction patterns of the θ' phase, and the orientation relationship between the θ' phase and matrix as follows: $[100]_{Al}//[100]_{S(S')}$, $[021]_{Al}//[010]_{S(S')}$ and $[012]_{Al}//[001]_{S(S')}$ [25]. The S phase is incoherent with the matrix, and hinders the movement of the dislocations. Figure 5(f) shows the diffraction pattern of the θ' phase, and the orientation relationship between the θ' phase and matrix is $[010]_{\theta'}//[001]_{Al}$ [25]. The θ' phase is semi-coherent with the matrix, has a larger coherent strain, which leads to a larger strengthening effect of the alloy. Therefore, the S phases and θ' phases in the T6I6 treated Al-Cu-Mg alloy can improve the mechanical properties of the alloy.

In the initial aging treatment, because the diffusivity and vacancy binding energy of Mg are greater than those of Cu, the S phase firstly precipitates in the supersaturated solid solution. When the aging treatment is interrupted at a low temperature, relatively few Mg atoms are precipitated from the alloy, and Cu atoms are continuously precipitated. The GPB zone and GP zone are more likely to be secondary precipitated in the alloy [27]. Increasing the temperature and prolonging the time of interrupted aging are more conducive to the nucleation of the secondary precipitates, leading to the coarsening of primary S phase. In the re-aging treatment, the primary S phase continues to grow and even coarsens, and the secondary GPB zone and GP zone gradually change into S phase and θ' phase, respectively.

The improvement of the mechanical properties of the T6I6 treated alloy is mainly due to the coexistence of fine and uniform S and θ' phases. The continuous precipitation of Cu atoms in the alloy will make the potential of the alloy close to that of pure Al [28], which can reduce the corrosion sensitivity of the alloy.

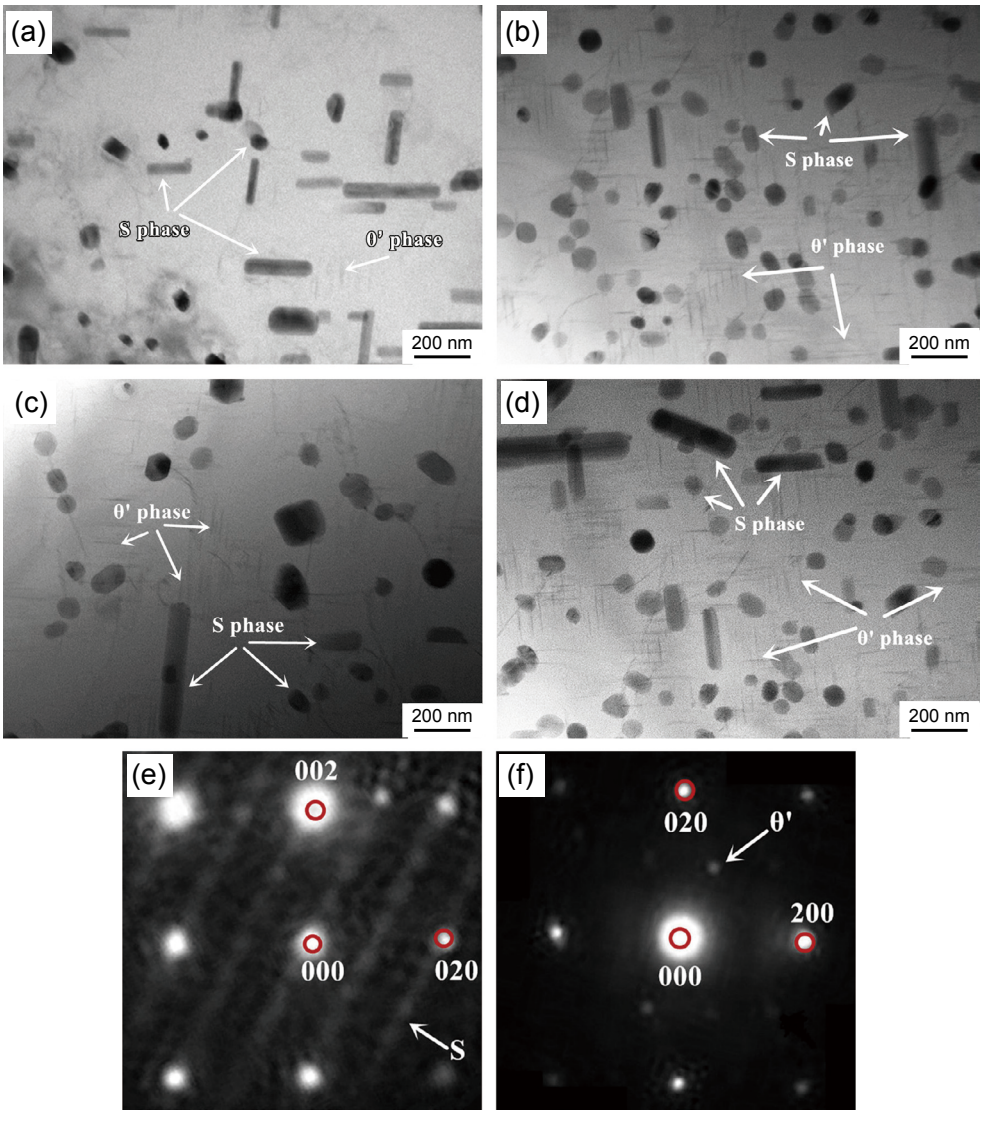


**Fig. 5: TEM images of O1 (a), O2 (b), O3 (c), and O4 (d) samples, and diffraction pattern of S (e) and θ' (f) phases**

## 5 Conclusions

(1) Properly increasing the interrupted aging temperature is beneficial to enhance the aging-hardening and strengthening effect of the alloy. The tensile strength and hardness of the alloy with optimal T6I6 process, i.e., initial aged at 180 °C for 2 h, interrupted aged at 90 °C for 30 min and re-aged at 170 °C for 4 h, are 443.6 MPa and 161.6 HV, respectively, the exfoliation corrosion rating is EA, and the intergranular corrosion depth is 105 μm.

(2) The secondary precipitation phenomenon can increase the strengthening phases in the T6I6 treated alloy. The improvement in the mechanical properties and corrosion resistance of the cast Al-Cu-Mg alloy is mainly due to the coexistence of fine and uniform S phase and θ' phase after T6I6 treatment.

## Acknowledgements

This work was financially supported by the Program for National Key Research and Development Plan (No. 2017YFB1104000), the National Natural Science Foundation of China (No. 51574167), the Liaoning Natural Science Foundation (No. 2021-MS-235), and the Science and Technology Program of Liaoning Provincial Department of Education (No. LJGD2020010).

## Conflict of interest

The authors declare that they have no conflict of interest.

## References

[1] Du A H, Wang W G, Gu X F, et al. The dependence of precipitate morphology on the grain boundary types in an aged Al-Cu binary alloy. Journal of Materials Science, 2021, 56(1): 781–791.
[2] Liu F, Liu Z Y, Liu M, et al. Analysis of empirical relation between microstructure, texture evolution and fatigue properties of an Al-Cu-Li alloy during different pre-deformation processes. Materials Science and Engineering A, 2019, 726: 309–319.
[3] Shi W N, Zhou H F, Zhang X F. High-strength and anti-corrosion of Al-Cu-Mg alloy by controlled ageing process. Philosophical Magazine Letters, 2019, 99(7): 235–242.
[4] Qi Z W, Cong B Q, Qi B J, et al. Microstructure and mechanical properties of double-wire plus arc additively manufactured Al-Cu-Mg alloys. Journal of Materials Processing Technology, 2018, 255: 347–353.
[5] Zainul H, Nur I T, Tuan Z. Characterization of 2024-T3: An aerospace aluminum alloy. Materials Chemistry and Physics, 2009, 113(2–3): 151–157.
[6] Barros A, Cruz C, Silva A P, et al. Length scale of solidification microstructure tailoring corrosion resistance and microhardness in T6 heat treatment of an Al-Cu-Mg alloy. Corrosion Engineering Science and Technology, 2020, 55(6): 471–479.
[7] Niu P L, Lia W Y, Lia N, et al. Exfoliation corrosion of friction stir welded dissimilar 2024-to-7075 aluminum alloys. Materials Characterization, 2019, 147: 93–100.
[8] Marceau R K W, Sha G, Lumley R N, et al. Evolution of solute clustering in Al-Cu-Mg alloys during secondary ageing. Acta Materialia, 2010, 58(5): 1795–1805.
[9] Gao N, Starink M J, Kamp N, et al. Application of uniform design in optimisation of three stage ageing of Al-Cu-Mg alloys. Journal of Materials Science, 2007, 42(12): 4398–4405.
[10] Ye L Y, Gu G, Zhang X M, et al. Dynamic properties evaluation of 2519A aluminum alloy processed by interrupted aging. Materials Science and Engineering A, 2014, 590(1): 97–100.
[11] Lumley R N, Polmear I J, Morton A J. Heat treatment of age hardenable aluminium alloys utilizing secondary precipitation. US Patent No. 7037391 B2, 2006-05-02.
[12] Xu X H, Deng Y L, Chi S Q, et al. Effect of interrupted ageing treatment on the mechanical properties and intergranular corrosion behavior of Al-Mg-Si alloys. Journal of Materials Research and Technology, 2020, 9(1): 230–241.
[13] Buha J, Lumley R N, Crosky A G, et al. Secondary precipitation in an Al-Mg-Si-Cu alloy. Acta Materialia, 2007, 55(9): 3015–3024.
[14] Chen Y, Weyland M, Hutchinson C R. The effect of interrupted aging on the yield strength and uniform elongation of precipitation-hardened Al alloys. Acta Materialia, 2013, 61: 5877–5894.
[15] Lumley R N, Polmear I J, Morton A J. Development of mechanical properties during secondary aging in aluminium alloys. Materials Science and Technology, 2005, 21(9): 1025–1032.
[16] Lumley R N, Polmear I J, Morton A J. Development of properties during secondary ageing of aluminium alloys. Materials Science Forum, 2003, 426–432(4): 303–308.
[17] Yin M J, Chen J H, Liu C H. Effect of interrupted aging treatment on mechanical properties and microstructure of AA2024 aluminum alloy. Transactions of Nonferrous Metals Society of China, 2015, 25(12): 3271–3281. (In Chinese)
[18] Li H, Pan D Z, Wang Z X, et al. Influence of T6I6 temper on tensile and intergranular corrosion properties of 6061 aluminum alloy. Acta Metallurgica Sinica, 2010, 46(4): 494–499. (In Chinese)
[19] Boag A, Taylor R J, Muster T H, et al. Stable pit formation on AA2024-T3 in a NaCl environment. Corrosion Science, 2010, 52(1): 90–103.
[20] Kurtulmus M. Experimental investigation and optimization of welding parameters on weld strength in friction stir spot welding of aluminum using Taguchi experimental design. Emerging Materials Research, 2020, 9(6): 662–667.
[21] Vidal C, Infante V. Optimization of FS welding parameters for improving mechanical behavior of AA2024-T351 joints based on Taguchi method. Journal of Materials Engineering and Performance, 2013, 22(8): 2261–2270.
[22] Xin F H, Liu W H, Song L, et al. Modification of inorganic binder used for sand core-making in foundry practice. China Foundry, 2020, 17(5): 341–346.
[23] Li H Z, Liu R M, Liang X P, et al. Effect of pre-deformation on microstructures and mechanical properties of high purity Al-Cu-Mg alloy. Transactions of Nonferrous Metals Society of China, 2016, 26(6): 1482–1490.
[24] Oltra R, Vuillemin B, Rechou F, et al. Effect of aeration on the microelectrochemical characterization of $Al_2Cu$ intermetallic phases. Electrochemical and Solid-State Letters, 2009, 12(12): C29–C31.
[25] Wang S C, Starink M J. Precipitates and intermetallic phases in precipitation hardening Al-Cu-Mg-(Li) based alloys. Acta Materialia, 2005, 50(4): 193–215.
[26] Wang S C, Starink M J. Two types of S phase precipitates in Al-Cu-Mg alloys. Acta Materialia, 2007, 55(3): 933–941.
[27] Kim I S, Song M Y, Kim J H, et al. Effect of added Mg on the clustering and two-step aging behavior of Al-Cu alloys. Materials Science and Engineering A, 2020, 798: 140123.
[28] Warner J S, Gangloff R P. Alloy induced inhibition of fatigue crack growth in age-hardenable Al-Cu alloys. International Journal of Fatigue, 2012, 42: 35–44.